Scaling of the F_2 Structure Function in Nuclei and Quark Distributions at $x > 1$

N. Fomin,[1,2] J. Arrington,[3] D. B. Day,[1] D. Gaskell,[4] A. Daniel,[5] J. Seely,[6] R. Asaturyan,[7,*] F. Benmokhtar,[8] W. Boeglin,[9] B. Boillat,[10] P. Bosted,[4] A. Bruell,[4] M. H. S. Bukhari,[5] M. E. Christy,[11] E. Chudakov,[4] B. Clasie,[6] S. H. Connell,[12] M. M. Dalton,[1] D. Dutta,[13,14] R. Ent,[4] L. El Fassi,[3] H. Fenker,[4] B. W. Filippone,[15] K. Garrow,[16] C. Hill,[1] R. J. Holt,[3] T. Horn,[8,4] M. K. Jones,[4] J. Jourdan,[10] N. Kalantarians,[5] C. E. Keppel,[4,11] D. Kiselev,[10] M. Kotulla,[10] R. Lindgren,[1] A. F. Lung,[4] S. Malace,[11] P. Markowitz,[9] P. McKee,[1] D. G. Meekins,[4] T. Miyoshi,[17] H. Mkrtchyan,[7] T. Navasardyan,[7] G. Niculescu,[18] Y. Okayasu,[17] A. K. Opper,[19] C. Perdrisat,[20] D. H. Potterveld,[3] V. Punjabi,[21] X. Qian,[14] P. E. Reimer,[3] J. Roche,[19,4] V. M. Rodriguez,[5] O. Rondon,[1] E. Schulte,[3] E. Segbefia,[11] K. Slifer,[1] G. R. Smith,[4] P. Solvignon,[3] V. Tadevosyan,[7] S. Tajima,[1] L. Tang,[4,11] G. Testa,[10] R. Trojer,[10] V. Tvaskis,[11] W. F. Vulcan,[4] C. Wasko,[1] F. R. Wesselmann,[21] S. A. Wood,[4] J. Wright,[1] and X. Zheng[1,3]

[1]*University of Virginia, Charlottesville, Virginia, USA*
[2]*University of Tennessee, Knoxville, Tennessee, USA*
[3]*Physics Division, Argonne National Laboratory, Argonne, Illinois, USA*
[4]*Thomas Jefferson National Laboratory, Newport News, Virginia, USA*
[5]*University of Houston, Houston, Texas, USA*
[6]*Massachusetts Institute of Technology, Cambridge, Massachusetts, USA*
[7]*Yerevan Physics Institute, Yerevan, Armenia*
[8]*University of Maryland, College Park, Maryland, USA*
[9]*Florida International University, Miami, Florida, USA*
[10]*Basel University, Basel, Switzerland*
[11]*Hampton University, Hampton, Virginia, USA*
[12]*University of Johannesburg, Johannesburg, South Africa*
[13]*Mississippi State University, Jackson, Mississippi, USA*
[14]*Duke University, Durham, North Carolina, USA*
[15]*Kellogg Radiation Laboratory, California Institute of Technology, Pasadena, California, USA*
[16]*TRIUMF, Vancouver, British Columbia, Canada*
[17]*Tohoku University, Sendai, Japan*
[18]*James Madison University, Harrisonburg, Virginia, USA*
[19]*Ohio University, Athens, Ohio, USA*
[20]*College of William and Mary, Williamsburg, Virginia, USA*
[21]*Norfolk State University, Norfolk, Virginia, USA*

(Received 20 August 2010; published 17 November 2010)

We present new data on electron scattering from a range of nuclei taken in Hall C at Jefferson Lab. For heavy nuclei, we observe a rapid falloff in the cross section for $x > 1$, which is sensitive to short-range contributions to the nuclear wave function, and in deep inelastic scattering corresponds to probing extremely high momentum quarks. This result agrees with higher energy muon scattering measurements, but is in sharp contrast to neutrino scattering measurements which suggested a dramatic enhancement in the distribution of the "superfast" quarks probed at $x > 1$. The falloff at $x > 1$ is noticeably stronger in ^{2}H and ^{3}He, but nearly identical for all heavier nuclei.

DOI: 10.1103/PhysRevLett.105.212502 PACS numbers: 25.30.Fj, 13.60.Hb, 24.85.+p

The quark structure of nuclei is extremely complex, and a detailed understanding of nuclei at the quark level requires the careful incorporation of nucleonic degrees of freedom and interactions as well as the dynamics of quarks and gluons. In inclusive electron scattering from nuclei, the cross section is characterized by the structure functions $F_1(\nu, Q^2)$ and $F_2(\nu, Q^2)$, where ν is the energy transfer and $-Q^2$ is the square of the four-momentum transfer. At high Q^2, the reaction is dominated by elastic scattering from quasifree quarks, and one can probe the momentum distribution of the quarks. In the Bjorken limit ($\nu, Q^2 \to \infty$), the quark mass and transverse momenta are negligible compared to the energy and momentum of the probe, and the scattering is sensitive only to the quark longitudinal momentum, where $x = Q^2/(2M\nu)$ is the fraction of the hadron's longitudinal momentum carried by the quark in the infinite momentum frame. In this deep inelastic scattering (DIS) limit, the structure functions exhibit scaling, i.e., $F_2(\nu, Q^2) \to F_2(x)$, becoming independent of Q^2 at fixed x, with $F_2(x)$ proportional to a charge-weighted sum of the quark momentum distributions in the target.

As one moves away from the Bjorken limit, there are deviations from perfect scaling. At finite Q^2, kinematical corrections yield a Q^2 dependence that can be large for low

Q^2 or large x. While these scaling violations have historically been called ''target mass'' corrections [1], they are in fact independent of the mass of the target for a quark of a given longitudinal momentum. At lower Q^2, there are also significant contributions from higher twist effects, e.g., structure due to quark-quark and quark-gluon correlations which appear most clearly as strong resonance structure. These scaling violating terms make extraction of the quark distributions most straightforward at high energies. QCD evolution yields an approximately logarithmic Q^2 dependence at all Q^2 values, but this is a true scale dependence of the parton distributions.

The early expectation was that the nuclear quark momentum distribution would be a convolution of the distribution of nucleons in a nucleus with the distribution of quarks in the nucleons. Contrary to these expectations, measurements of inclusive scattering from nuclei showed a 10%–20% suppression of high momentum quarks ($0.3 < x < 0.8$) in heavy nuclei [2], demonstrating that the quark distributions in nuclei are not simply a sum of the proton's and neutron's quark distributions.

The quark distribution at $x > 1$ is extremely small in the convolution model, as the nucleon quark distributions fall rapidly as $x \rightarrow 1$ and there are very few fast nucleons available to boost the quarks to $x > 1$. The bulk of these 'superfast' quarks come from nucleons above the Fermi momentum, which are generated by the repulsive core of the N-N interaction; they reflect the short-range correlations in the ground state nuclear wave function [3,4]. Exotic configurations, such as 6-quark bags, may provide an even more efficient mechanism for generating very high momentum quarks, as the quarks from two nucleons can more freely share momentum [2,4]. It is clear that a holistic explanation of DIS from nuclei must describe the structure functions in the full kinematic range, and data at $x > 1$ are necessary to illuminate the presence of short-range structure in nuclei.

There are only two high energy measurements thus far for $x \gtrsim 1$, and they yield dramatically different results. Muon scattering data from the BCDMS Collaboration [5] for Q^2 from 52–200 GeV^2 show a rapid falloff in $F_2(x)$. They find $F_2(x) \propto \exp(-sx)$ with $s = 16.5 \pm 0.6$ for $0.75 < x < 1.05$, which suggests the need for relatively modest contributions from short-range correlations. Neutrino scattering measurements from the CCFR Collaboration [6] at $Q^2 = 125$ GeV^2 yield $s = 8.3 \pm 0.7$ for $0.75 < x < 1.2$, which has been interpreted as an indication of exceptionally large strength from short-range correlations or the need for other, more exotic, contributions. However, both measurements have important limitations: CCFR had to make significant corrections due to the poor resolution on their reconstructed x value, while BCDMS was only able to extract F_2 up to $x = 1.05$. It is unclear if this is sufficient to make meaningful comparisons to model predictions of short-range structure in nuclei, as this is not expected to dominate until $x \gtrsim 1.2$ [7,8]. More extensive measurements have been made at lower energies, but they have been limited to $x \approx 1$ [9,10] or $Q^2 < 5$ GeV^2 [11–13].

We present the results of JLab E02-019, which made new measurements of inclusive scattering from nuclei, covering an expanded range in x and Q^2. Data were taken for few-body and heavy nuclei, covering both the region of the EMC effect [14] and $x > 1$. The measurement was performed in Hall C at the Thomas Jefferson National Accelerator Facility in 2004. A continuous wave electron beam of 5.766 GeV and current of ≈ 80 μA was supplied. Electrons scattered from the target were detected using the High Momentum Spectrometer (HMS) at $\theta = 18°$, $22°$, $26°$, $32°$, $40°$, and $50°$, corresponding to $2 \lesssim Q^2 \lesssim 9$ GeV^2. Data were taken on cryogenic ^{2}H, ^{3}He, ^{4}He targets, solid Be, C, Cu, and Au targets, as well as Al targets used to measure and correct for the contribution from the walls of the cryogenic target cells.

Electrons were selected using the HMS gas Čerenkov and electromagnetic calorimeter detectors with efficiencies of >98% and >99.7%, respectively, and negligible pion contamination. Data were also taken with the HMS in positive polarity to determine the contribution from charge-symmetric processes. The systematic error associated with positron subtraction was negligible except at the largest Q^2 values, where it is under 2%. The uncertainty due to the spectrometer acceptance is 1.4%.

The largest sources of systematic uncertainty at high x come from the beam energy (0.05%), HMS central momentum (0.05%), and angle (0.5 mrad) settings. The associated uncertainties are typically small (1%–2% for $x < 1$) except for very large x, where the uncertainty can reach 4%–6%. The correction and systematic uncertainty arising from subtraction of the aluminum end caps (cryogenic targets only) also grows with increasing x values, yielding an uncertainty of 0.3%–2.4%. The cross sections also had to be corrected for radiative and Coulomb effects, which yield systematic uncertainties of 1.4%, and <2%, respectively. The Coulomb distortion of the electron wave function by the electrostatic field of the nucleus was corrected for using the local effective momentum approximation method [15]. For the radiative corrections, the energy peaking approximation method of Mo and Tsai [16] was found to be insufficient for thick targets, and the full 2D integral over energies of the radiated photon in the initial and final states [17] was calculated. In this approach (detailed in Ref. [18]), a complete calculation of the Mo-Tsai formula for external and internal effects is performed, using equivalent radiator approximation to simultaneously calculate the internal and external radiative corrections. Complete details of the analysis can be found in Ref. [19]. The total systematic uncertainty on the extracted cross sections is below 4% for $x < 1$, and up to 6% in the $1 < x \lesssim 2$ range.

The structure function per nucleon, $F_2(\nu, Q^2)$, is extracted from the measured cross section as follows:

$$F_2 = \frac{d^2\sigma}{d\Omega dE} \times \frac{\nu}{\sigma_{\text{Mott}}\{1 + 2\tan^2(\theta/2)[(1 + \nu^2/Q^2)/(1 + R)]\}}, \quad (1)$$

with $R \equiv \sigma_L/\sigma_T$, and is parametrized as $R = (0.32\ \text{GeV}^2)/Q^2$ [9] with $\delta R/R = 50\%$, yielding an additional uncertainty of $\lesssim 1\%$ in F_2.

Scaling of the proton structure functions has been observed over a large kinematic range in high energy inclusive scattering. Based on these measurements, the DIS region is often taken to be $W^2 > 4\ \text{GeV}^2$, $Q^2 > 1\ \text{GeV}^2$, where $W^2 = M_p^2 + 2M_p\nu - Q^2$ is the square of the invariant mass of the undetected hadronic system and M_p is the proton mass. It has been shown that scaling violations are reduced when one examines F_2 at fixed $\xi = 2x/(1 + r)$ [20], where $r = \sqrt{1 + Q^2/\nu^2}$. ξ is equivalent to x in the Bjorken limit, but when examining scaling at fixed ξ, rather than fixed x, the observed scaling behavior extends to lower W^2 [12,13], corresponding to larger ξ values. This improved scaling can be seen clearly in Fig. 1, where the upper sets of curves show F_2 for carbon plotted against x (red squares) and ξ (blue circles) for all Q^2 values. The extended ξ scaling of the nuclear structure function, seen to begin above 3–4 GeV^2, may allow access to quark distributions for $\xi \gtrsim 1$ [21,22]. Beyond the empirical observation that it yields reduced scaling violations, ξ is the variable representing the quark momentum fraction on the light cone, and also arises naturally from the operator product expansion [1].

We compare our data to higher Q^2 measurements, using a partonic framework to look for deviations from the scaling picture. Rather than simply examining F_2 as a function of ξ, as was done previously, we account for the kinematical scaling violations using the prescription of Ref. [1] [Eq. (23)] and study the scaling of $F_2^{(0)}(\xi, Q^2)$:

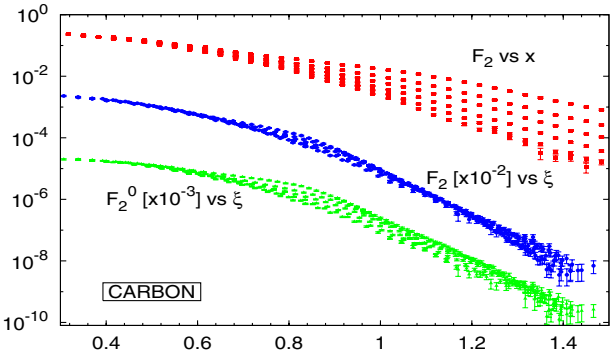

FIG. 1 (color online). F_2 for the E02-019 carbon data ($2.3 \lesssim Q^2 \lesssim 9\ \text{GeV}^2$) as a function of x (top set of points) and ξ (middle), and $F_2^{(0)}$ vs ξ (bottom). In each case, the higher points correspond to the smaller scattering angles.

$$\frac{x^2}{\xi^2 r^3} F_2^{(0)}(\xi, Q^2) = F_2(x, Q^2) - \frac{6M^2x^3}{Q^2r^4} h_2(\xi, Q^2) - \frac{12M^4x^4}{Q^4r^5} g_2(\xi, Q^2), \quad (2)$$

where $h_2(\xi, Q^2) = \int_\xi^A u^{-2} F_2^{(0)}(u, Q^2)du$ and $g_2(\xi, Q^2) = \int_\xi^A v^{-2}(v - \xi)F_2^{(0)}(v, Q^2)dv$. In the operator product expansion, it is $F_2^{(0)}(\xi, Q^2)$, rather than $F_2(x, Q^2)$, that should be independent of Q^2 in the absence of QCD evolution and higher twist. One could incorporate these effects into a partonic model for F_2, rather than extracting an "idealized" scaling function, but the improved scaling in $F_2^{(0)}$ makes it easier to directly compare different data sets.

To calculate h_2 and g_2, we use a factorized model for $F_2^{(0)}(\xi, Q^2)$, with a common Q^2 dependence for all targets and a simple fit to $F_2^{(0)}(\xi, Q_0^2)$ for each nucleus. In the partonic picture, the Q^2 dependence should come only from QCD evolution. Because we cannot determine QCD evolution without knowing the partonic structure, we fit the Q^2 dependence of the world's data (shown in Fig. 2), excluding our lower Q^2 points, at several ξ values to a functional form chosen to be consistent with evolution. This is used to scale our new data to $Q_0^2 = 7\ \text{GeV}^2$, and we obtain a fit for $F_2^{(0)}(\xi, Q_0^2)$ from a subset of these data, chosen to minimize contributions from quasielastic

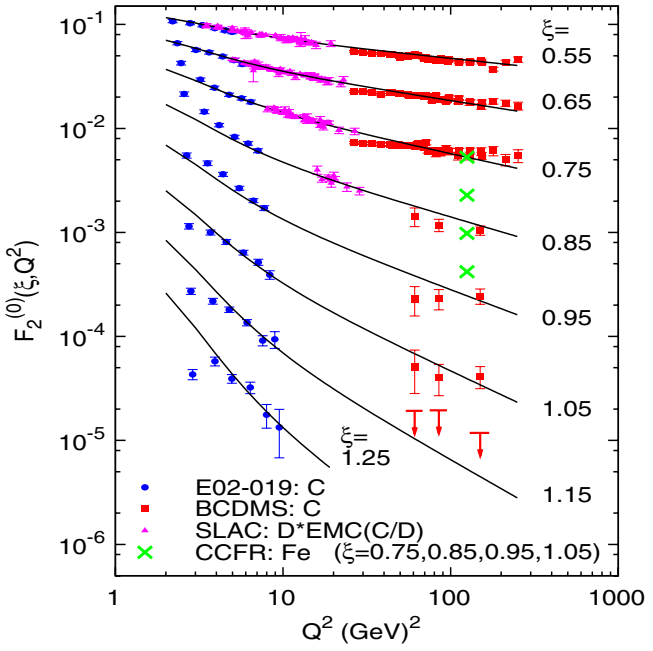

FIG. 2 (color online). $F_2^{(0)}$ vs Q^2 for fixed ξ value. For this work and BCDMS, the carbon data are shown, while the SLAC points are carbon pseudodata taken from measurements on deuterium. The solid curves are the global fit, the short horizontal red lines show the BCDMS $\xi = 1.15$ upper limit, and the green crosses show the falloff between $\xi = 0.75$ and 1.05 based on the CCFR iron data (see text for details).

scattering. This simple fit provides a reasonable description of the global data set (see Fig. 2), with deviations at low Q^2, in particular, near the quasielastic peak ($\xi \approx 0.85$) and for the largest values of ξ. The h_2 and g_2 terms yield corrections of up to 15% at the lower Q^2 values, but $\lesssim$ 5% for $Q^2 > 5$ GeV^2. We estimate the model dependence in the extraction of $F_2^{(0)}$ to be $\lesssim 2\%$.

Figure 1 shows $F_2^{(0)}$ vs ξ (green triangles), which has somewhat greater Q^2 dependence at large ξ than the uncorrected structure function F_2 (blue circles). The main difference between ξ scaling of F_2 and $F_2^{(0)}$ is the factor $x^2/(\xi^2 r^3)$ multiplying the leading term in Eq. (2), as h_2 and g_2 are relatively small. Neglecting this prefactor introduces an additional Q^2 dependence that approximately cancels the QCD evolution, resulting in an artificially small Q^2 dependence in the naive ξ-scaling analysis.

Figure 2 shows the carbon results for $F_2^{(0)}(\xi, Q^2)$, scaled to fixed values of ξ using our global fit. The SLAC points are deuterium data [23], multiplied by the SLAC E139 [24] fit to the carbon-to-deuteron structure function ratio, yielding carbon pseudodata to provide a continuous Q^2 range for lower ξ values. For all data sets, $F_2^{(0)}$ is extracted from the measured structure functions using the global fit to calculate g_2 and h_2. For $\xi \leq 0.75$, where the high Q^2 data determine the evolution, our data are in excellent agreement with this Q^2 dependence down to $Q^2 =$ 3 GeV^2. The observed Q^2 dependence grows slowly with ξ over this region, and with a continued increase at higher ξ values, our highest Q^2 measurements are consistent with SLAC and BCDMS. For large ξ values at low Q^2, our data deviate from this Q^2 dependence due to higher twist contributions, especially in the vicinity of the quasielastic peak ($\xi \approx 0.85$).

The CCFR measurement did not explicitly extract values of F_2, but obtained a fit to the falloff at large ξ. We illustrate this falloff by normalizing to our global fit at $\xi =$ 0.75 and applying the CCFR ξ dependence to extract $F_2^{(0)}$ at $\xi = 0.75$, 0.85, 0.95, and 1.05, shown as green crosses. This behavior is clearly inconsistent with the overall behavior of the structure function extracted from electron and muon scattering. The BCDMS data exhibit somewhat unusual behavior at large ξ. Above $\xi = 0.65$, the BCDMS data show little or no Q^2 dependence, even though one expects noticeable QCD evolution.

To quantitatively examine the falloff of our structure function at large ξ, we perform a fit similar to BCDMS and CCFR. We take the data from a fixed scattering angle, use the global fit to scale to a fixed Q^2 value (corresponding to $\xi = 1.1$), and fit $F_2^{(0)}(\xi, Q^2)$ to $\exp(-s\xi)$ for $1 < \xi <$ 1.25. The lower ξ limit is chosen to avoid regions where the quasielastic peak leads to noticeable deviations from scaling at low Q^2, and the upper ξ limit is chosen so that there are data covering the full ξ range for all targets and Q^2 values. We take the slope extracted from the 40° data ($Q^2 = 7.35$ GeV^2) as the main result, as this is the largest Q^2 value with high statistics over the full ξ range. Data at smaller angles are used to examine the Q^2 dependence of the result.

TABLE I. Extracted values of the slopes for all nuclei. The uncertainties include statistics and systematics; the latter are typically ~0.4 and dominate the uncertainty.

A	$Q^2 = 2.79$	3.75	4.68	5.95	7.35
2	14.7 ± 0.6	16.6 ± 0.5	17.1 ± 0.5	17.5 ± 0.7	16.8 ± 0.8
3	15.1 ± 0.6	15.6 ± 0.5	16.6 ± 0.6	16.4 ± 0.7	17.4 ± 0.9
4	14.8 ± 0.5	14.7 ± 0.5	15.1 ± 0.5	15.1 ± 0.5	14.8 ± 0.6
9	14.7 ± 0.5	14.6 ± 0.4	14.8 ± 0.4	15.0 ± 0.4	15.0 ± 0.5
12	14.7 ± 0.5	14.3 ± 0.4	14.9 ± 0.4	14.5 ± 0.4	15.0 ± 0.5
64	13.8 ± 0.5	13.7 ± 0.4	14.2 ± 0.4	13.9 ± 0.4	14.1 ± 0.5
197	13.5 ± 0.6	13.6 ± 0.5	13.9 ± 0.5	13.9 ± 0.5	14.3 ± 0.7

The extracted slopes are shown in Table I and Fig. 3. Above 4 GeV^2, there is no systematic Q^2 dependence, and at lower Q^2, only the ^{2}H and ^{3}He results change significantly. We observe nearly identical behavior in the high-ξ falloff for all nuclei except ^{2}H and ^{3}He, which have a larger slope and thus a steeper falloff with ξ.

We obtain $s = 15.0 \pm 0.5$ for carbon, $s = 14.1 \pm 0.5$ for copper (our closest nucleus to the CCFR iron target), showing that the large difference between BCDMS and CCFR is not related to the difference in target nuclei. Note that BCDMS and CCFR extract slopes from $F_2(x)$ instead of $F_2^{(0)}(\xi)$, although the difference would increase their slopes by less then 0.5 (0.1) for the BCDMS (CCFR). Further complicating direct comparison is the fact that none of these experiments cover the same ξ range. For our new data, variations in the ξ limits of 0.05–0.1 can change the extracted slope by 0.5–1.0.

We have focused on heavier nuclei for comparison to BCDMS and CCFR, but have also obtained a significantly

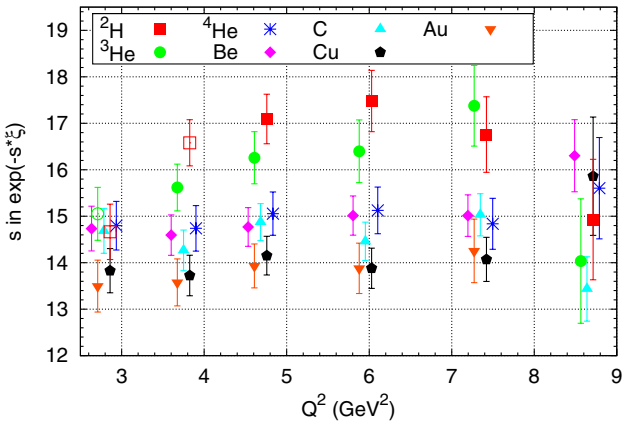

FIG. 3 (color online). The slope s in $\exp(-s\xi)$ as a function of Q^2. The targets are offset in Q^2 for visibility. Open symbols for ^{2}H and ^{3}He at low Q^2 are cases where the kinematic limit for the nucleus ($x \approx A$) corresponds to $\xi \lesssim 1.25$.

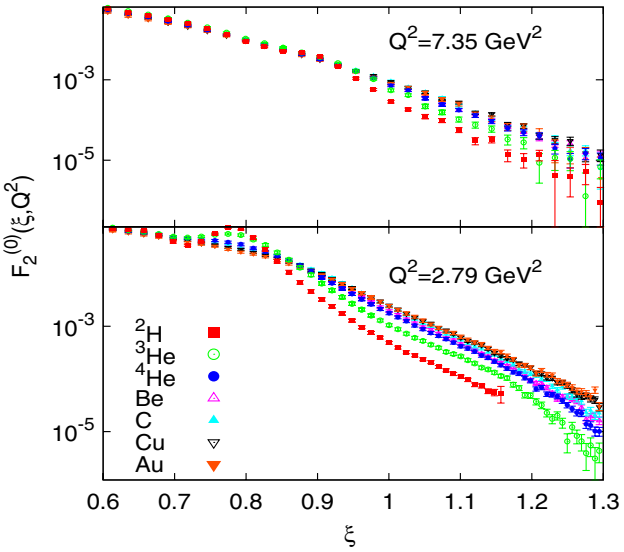

FIG. 4 (color online). The extracted scaling structure function per nucleon for all nuclei at $Q^2 = 2.79$ and 7.35 GeV^2. The deuteron data are kinematically limited to $x < 2$, corresponding to $\xi \lesssim 1.15$ for the low Q^2 setting.

expanded body of data for light nuclei, shown in Fig. 4. At low Q^2, the light nuclei show a clear quasielastic peak, while at higher Q^2 the peak is almost entirely washed out. For heavier nuclei, the extracted scaling function per nucleon is nearly identical at all ξ values. However, for ^{2}H and ^{3}He, there is a significant reduction in strength for $\xi \gtrsim 1$, which is observed at all Q^2 values.

In summary, we have made extensive measurements of the large ξ structure functions for Q^2 from 2–9 GeV^2. We have extracted the scaling structure function, $F_2^{(0)}(\xi, Q^2)$, and shown that it is consistent with a nearly logarithmic Q^2 dependence over a significant range of ξ and Q^2. These new data do not show a need for extremely large contributions from short-range correlations or other, more exotic, short-range structures, as suggested by the CCFR result. The large ξ behavior of our data is consistent with the BCDMS results, but our results extend to significantly higher ξ values, where one expects to be most sensitive to short-range structure [4,8,25]. The new data, covering a range of nuclei at large ξ, can be used to directly constrain calculations of the effect of short-range correlations or multiquark configurations in our kinematic regime for a wide range of nuclei. A future 12 GeV JLab measurement will double the Q^2 range for these ξ values, moving to a region where we can directly extract the parton distributions of the superfast quarks in nuclei.

We thank the JLab technical staff and accelerator division for their contributions. This work supported in part by the NSF and DOE, including Grant No. NSF-0244899 and DOE Contracts No. DE-FG02-96ER40950, No. DE-AC02-06CH11357, and No. DE-AC05-06OR23177 under which JSA, LLC operates JLab, and the South African NRF.

*Deceased.

[1] I. Schienbein *et al.*, J. Phys. G **35**, 053101 (2008).
[2] D. F. Geesaman, K. Saito, and A. W. Thomas, Annu. Rev. Nucl. Part. Sci. **45**, 337 (1995).
[3] L. L. Frankfurt, M. I. Strikman, D. B. Day, and M. Sargsyan, Phys. Rev. C **48**, 2451 (1993).
[4] M. M. Sargsian *et al.*, J. Phys. G **29**, R1 (2003).
[5] A. Benvenuti *et al.* (BCDMS Collaboration), Z. Phys. C **63**, 29 (1994).
[6] M. Vakili *et al.* (CCFR Collaboration), Phys. Rev. D **61**, 052003 (2000).
[7] J. Rozynek and M. C. Birse, Phys. Rev. C **38**, 2201 (1988).
[8] L. L. Frankfurt and M. I. Strikman, Phys. Rep. **160**, 235 (1988).
[9] P. Bosted *et al.*, Phys. Rev. C **46**, 2505 (1992).
[10] J. Arrington *et al.*, Phys. Rev. C **53**, 2248 (1996).
[11] D. B. Day *et al.*, Phys. Rev. Lett. **43**, 1143 (1979).
[12] B. W. Filippone *et al.*, Phys. Rev. C **45**, 1582 (1992).
[13] J. Arrington *et al.*, Phys. Rev. C **64**, 014602 (2001).
[14] J. Seely *et al.*, Phys. Rev. Lett. **103**, 202301 (2009).
[15] A. Aste, C. von Arx, and D. Trautmann, Eur. Phys. J. A **26**, 167 (2005).
[16] L. W. Mo and Y.-S. Tsai, Rev. Mod. Phys. **41**, 205 (1969).
[17] S. Stein, W. B. Atwood, E. D. Bloom, R. L. A. Cottrell, H. DeStaebler, C. L. Jordan, H. G. Piel, C. Y. Prescott, R. Siemann, and R. E. Taylor, Phys. Rev. D **12**, 1884 (1975).
[18] S. R. Dasu, Ph.D. thesis, University of Rochester, 1988.
[19] N. Fomin, Ph.D. thesis, University of Virginia, 2007, arXiv:0812.2144.
[20] O. Nachtmann, Nucl. Phys. **B63**, 237 (1973).
[21] J. Arrington, R. Ent, C. E. Keppel, J. Mammei, and I. Niculescu, Phys. Rev. C **73**, 035205 (2006).
[22] W. Melnitchouk, R. Ent, and C. Keppel, Phys. Rep. **406**, 127 (2005).
[23] L. W. Whitlow, E. M. Riordan, S. Dasu, S. Rock, and A. Bodek, Phys. Lett. B **282**, 475 (1992).
[24] J. Gomez *et al.*, Phys. Rev. D **49**, 4348 (1994).
[25] O. Benhar, S. Fantoni, G. I. Lykasov, and N. V. Slavin, Phys. Rev. C **57**, 1532 (1998).